Pseudogap and charge ordering in a large-bandwidth electron-doped manganite

R. Bindu,[1] Ganesh Adhikary,[1] Nishaina Sahadev,[1] N. P. Lalla,[2] and Kalobaran Maiti[1,*]

[1]*Department of Condensed Matter Physics and Materials Science, Tata Institute of Fundamental Research, Homi Bhabha Road, Colaba, Mumbai-400 005, India*

[2]*UGC-DAE Consortium for Scientific Research, University Campus, Khandawa Road, Indore-452 017, India*

(Received 23 June 2011; published 29 August 2011)

We study the origin of complex phase transitions in an electron-doped manganite, $La_{0.2}Sr_{0.8}MnO_3$, using high-resolution photoemission spectroscopy and transmission electron microscopy. The results reveal evidence of phase coexistence and charge ordering in an intermediate temperature range unexpected in this high bandwidth system. The charge ordering nucleates above the phase transition temperature of 265 K, indicating a precursor effect. The high-resolution photoemission spectra exhibit unusual chemical potential shift and persistence of quasiparticles within the insulating phase below 265 K, where the charge-ordered phase dominates and hysteresis is observed in the resistivity. These results provide insight in the study of correlated electron systems exhibiting complex behaviors.

DOI: 10.1103/PhysRevB.84.052407 PACS number(s): 75.25.Dk, 68.37.Lp, 75.47.Lx, 79.60.Bm

The study of correlated electron systems has drawn immense attention during the past few decades following the discovery of properties such as high-temperature superconductivity, colossal magnetoresistance, heavy fermion behavior, etc. It is realized that the interplay of charge, spin, orbital, and lattice degrees of freedom leads to complexities in their properties. Manganites are ideal examples of the most complex systems, exhibiting properties such as colossal magnetoresistance, multiferroicity, electronic phase separation, charge, spin, and orbital ordering, etc.[1] Sr-doped $LaMnO_3$ (LSMO) has a large e_g bandwidth and is often considered as a canonical system, where the coexistence of ferromagnetism and metallicity can be explained using a double-exchange (DE) model. Later, it was pointed out[2] that electron-phonon coupling needs to be considered for a quantitative understanding of the effect as observed in superconductivity,[3] the charge-density-wave state,[4] etc.

In manganites, the bandwidth increases with an increase in the Mn-O-Mn bond angle, which is close to 180° in an electron-doped composition, $La_{0.2}Sr_{0.8}MnO_3$ (with a cubic structure at 300 K). $La_{0.2}Sr_{0.8}MnO_3$ exhibits interesting phase transitions—cubic to tetragonal, paramagnetic to *C*-type-antiferromagnetic, and metal to insulator—all occurring at ∼265 K.[5,6] Recent studies[7] showed the thermal evolution of the distortion of MnO_6 octahedra to follow the changes in resistivity and the existence of a finite band gap in the ground state, although the linear specific heat is high in this compound. Despite numerous studies, the origins of such complex behavior often observed in various correlated electron systems are not clear.

Here, we employed high-resolution photoemission spectroscopy (PES) and transmission electron microscopy (TEM) to probe the microscopic picture across the phase transition. A sample with a large grain size was prepared by long sintering; its high quality is manifested in the scanning electron microscopic data and other characterizations.[7,8] TEM measurements were carried out using a double-tilt liquid-nitrogen-based low-temperature holder (GATAN-636MA) in a Tecnai G2-20 TEM operating at 200 kV. For PES measurements, we used a Gammadata Scienta analyzer (R4000) and monochromatized photon sources: Al $K\alpha$, $h\nu = 1486.6$ eV, and He I, $h\nu = 21.2$ eV, with an energy resolution of 300 and 2 meV, respectively.

A TEM analysis at 300 K exhibited a cubic structure, as expected. As the temperature was reduced, two distinctly different spatial regions appeared below 260 K. A representative case is shown in Fig. 1(a) by different contrasts marked I and II in the 190-K micrograph (the region at the top right-hand corner corresponds to a different grain). Region I dominates until 190 K and then gradually reduces at lower temperatures, with a subsequent growth of region II. Approximately 90% of the sample converts into region II at ∼100 K: The estimation is done based on several high-resolution micrographs covering the entire grain—the ones shown in the figure represent a small portion of the grain of size ∼4 μm—as one micrograph of the whole grain will not have enough resolution to visualize the features. Once the sample transformed to the phase of region II, it remains dominant on heating until ∼260 K, indicating its intimate relationship to the observed hysteresis in resistivity.[7]

The selected-area diffraction (SAD) pattern of region II shown in Fig. 1(d) exhibits elliptical spots due to two closely spaced spots arising from twinned microstructures—a high-resolution micrograph shown in the inset of Fig. 1(b) manifests vertical stripes representing nearly equal width twins (∼10 nm). The SAD pattern of region I at 100 K [see Fig. 1(c)] unveils distinct superlattice spots near the fundamental ones representing the charge-ordered (CO) phase predicted earlier via sound velocity measurements,[9] providing a direct demonstration of the occurrence of the CO phase in large bandwidth systems. All the fundamental spots could be labeled based on the cubic unit cell ($Pm3m$, lattice parameter, $a = 3.8$ Å). The superlattice spots are found to be along the [110] and [1$\bar{1}$0] directions. The separations AB (=0.0375 Å^{-1}; periodicity = 27 Å) and AC (= 0.36575 Å^{-1}; periodicity = 2.7 Å) indicate that the charge ordering is commensurate, involving ten unit cells. With an increase in temperature, the superlattice spots gradually lose their sharpness, as shown in Fig. 1(e). The signature of the superlattice structure appears to persist even above 265 K. The diffracted peak intensity varies approximately as N^2

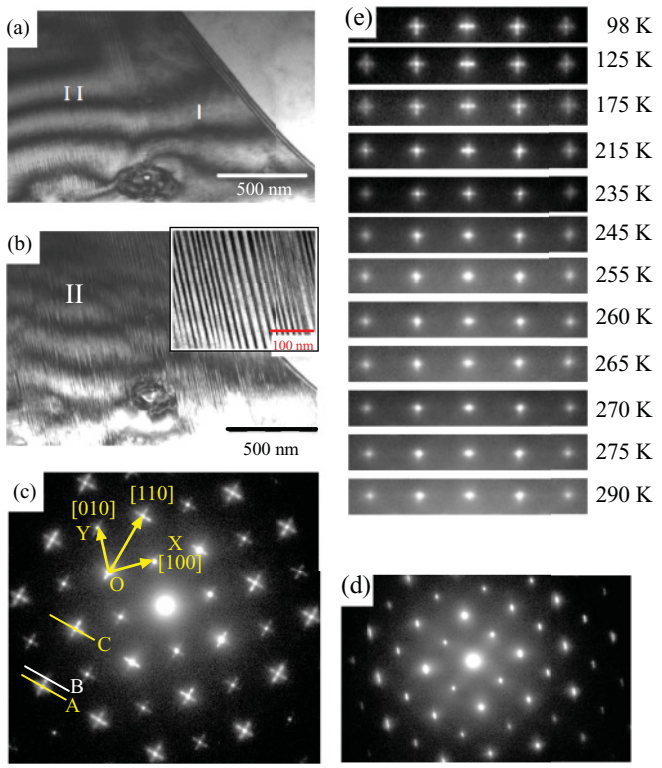

FIG. 1. (Color online) TEM micrographs at (a) 190 K and (b) 100 K. The inset in (b) shows a high-resolution micrograph of region II. SAD pattern at 100 K of (c) region I and (d) region II. (e) Temperature evolution of the SAD pattern of region I.

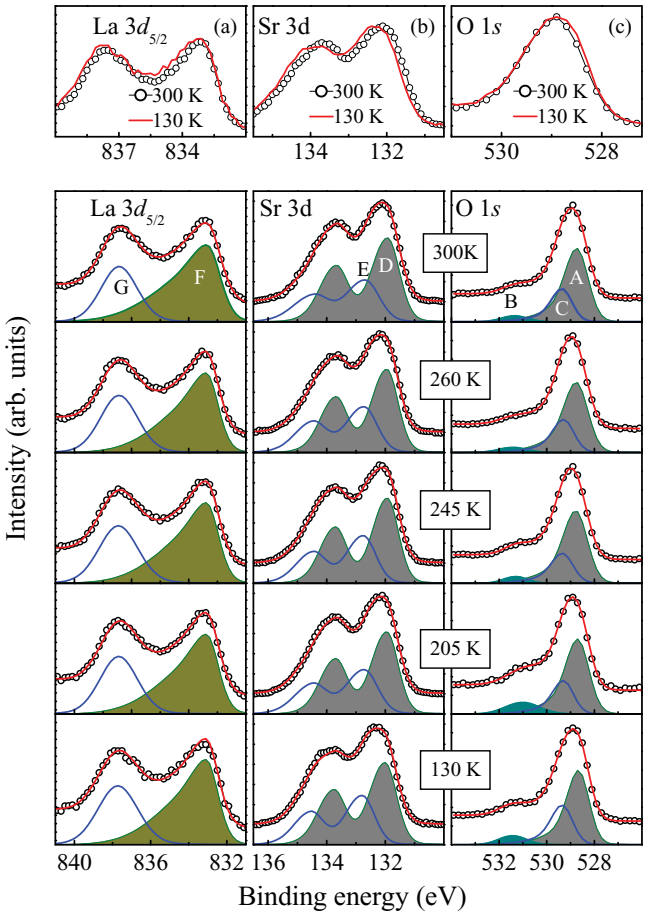

FIG. 2. (Color online) (a) La $3d_{5/2}$, (b) Sr $3d_{5/2}$, and (c) O $1s$ peaks at different temperatures. The top panel show the spectra at 300 K (symbols) and 130 K (lines) superimposed. The bottom panels show the fit to the experimental spectra (symbols).

(N = no. of unit cells involved in the CO phase) and the width as $1/N$. The superlattice spots are less prominent at higher temperatures, thus indicating a short-ranged CO phase above the phase transition temperature similar to the precursor effect observed in underdoped cuprate superconductors and magnetic systems.[10] Interestingly, cuprates also exhibit a striped phase.[11]

In order to investigate the phenomena microscopically, we probe the electronic structure with high-resolution photoemission spectroscopy. The core-level spectra shown in Fig. 2 exhibit multiple features and evolution with temperature. The La $3d_{5/2}$ signal exhibits two distinct features—cooling leads to a shift toward higher binding energies. The Sr $3d$ spectra seem anomalous—the intensity ratio of the spin-orbit split $3d_{3/2}$ and $3d_{5/2}$ signals does not follow the multiplicity ratio of 2 : 3. The energy shift with temperature is similar to the La $3d$ case. In contrast, the O $1s$ spectra exhibit an increase in intensity at ~528.5 eV with a decrease in temperature, although the edge at the higher binding energy side remains unchanged.

To estimate the energy shifts, we fit the core-level spectra with a set of asymmetric peaks[12] (see the bottom panels of Fig. 2). The peaks labeled F and G, representing the well-screened (the La $3d$ hole is screened by a ligand electron via charge transfer) and poorly screened (the La $3d$ hole is not screened) final states, fit the La $3d_{5/2}$ spectra well at all temperatures. For the Sr $3d$ spectra, it was necessary to take at least two sets (D and E) of the spin-orbit split features to derive the experimental spectra. Similar to the La $3d$ case, the set E can be attributed to charge-transfer satellites as found in other systems.[13,14] The O $1s$ spectra exhibit a weak (<2% of the signal) feature B at 531.5 eV due to sample surface and grain-boundary impurities, suggesting a good quality sample; the remaining part was fitted with peaks A and C, considering two types of Mn-O bond lengths,[6,7] leading to a different Madelung potential. The simulated spectra provide a good representation of the experimental spectra. The results of these fits are summarized in Fig. 4.

The Mn $2p$ spectra shown in Fig. 3 exhibit well-screened $2p_{3/2}$ and $2p_{1/2}$ features at ~642 and 653 eV, and corresponding satellites at ~652.5 and 663.5 eV, respectively. The $2p_{3/2}$ spectra exhibit a signature of three distinct features [see Fig. 3(b)]. The 640.8-eV feature can be attributed to the photoemission signal from Mn^{3+}, with the Mn^{4+} photoemission signal appearing at higher binding energies.[15] Such a distinct signature of multiple valency even in the metallic phase is often observed in early transition-metal oxides presumably due to a large charge-transfer energy.[16] The intensity ratio of these features matches well with the composition; the peak position of these two features will provide independent information about different Mn valency sites.

Based on the dependence of eigenenergies of the photoexcited states on various parameters,[17] the binding energy shift ($\Delta\epsilon$) can be expressed as $\Delta\epsilon = \Delta\mu + \Delta V_M + \Delta Q + \Delta E_R +$

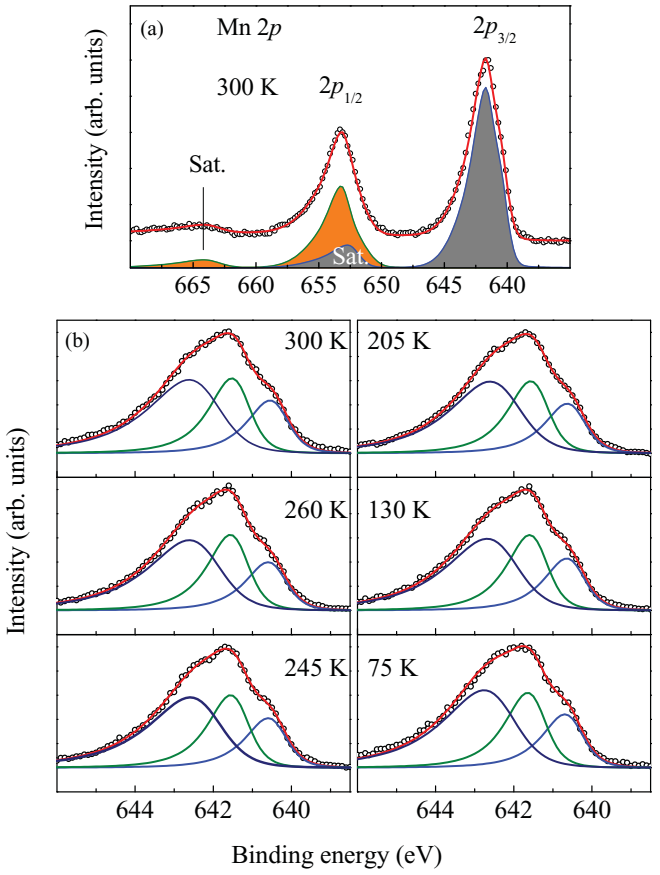

FIG. 3. (Color online) (a) Mn 2p spectra at 300 K. (b) The spectra (symbols) at different temperatures are fitted with three peaks (lines). The line superimposed on the symbols represents the total simulated Mn 2$p_{3/2}$ spectra.

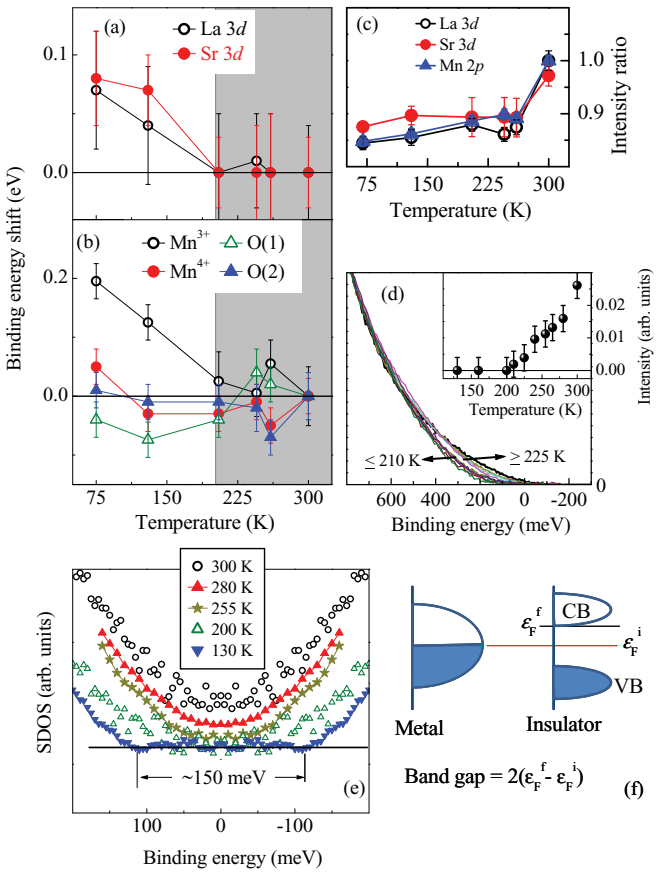

FIG. 4. (Color online) Binding energy shift in (a) La 3d and Sr 3d and (b) Mn 2p and O 1s spectra. (c) The intensity ratio of the main peak to the satellite with temperature. (d) High-resolution valence band and (e) the symmetrized spectra at different temperatures. The inset of (d) shows the intensity at the Fermi level as a function of temperature. (f) Schematic showing the shift of the Fermi level due to the metal-insulator transition in an electron-doped case.

ΔS, where μ is the chemical potential, V_M is the Madelung potential, Q is the valency, E_R is the relaxation energy, and S is the screening potential. Sr^{2+} and La^{3+} are highly stable ionic configurations. Therefore, the Sr 3d and La 3d energy shifts shown in Fig. 4(a) manifest the chemical potential shift as the other terms are insignificant here. The energy shifts in the Mn 2p and O 1s spectra shown in Fig. 4(b) are somewhat different from those in Fig. 4(a). While the energy shift of the Mn^{3+} 2p signals follow the trend observed for La and Sr core levels, the Mn^{4+} 2p and O 1s levels do not show a significant shift with temperature, indicating compensation for the chemical potential shift by some other parameter. Since, the Mn-O bond length exhibits an anomalous change with temperature,[7] such an anomaly can be attributed to a change in the Madelung potential at the Mn^{4+} and O sites. This is also manifested by a larger shift in the Mn^{3+} case.

The chemical potential shift due to an insulator-to-metal transition is shown schematically in Fig. 4(f). In the metallic phase, the valence band is partially filled and the chemical potential will remain almost unchanged in the temperature range studied. At the onset of the insulating phase, a gap opens up at the Fermi level. In a perfect crystal (no impurity or defect), the chemical potential may be found at the middle of the band gap—there is no chemical potential shift due to the metal-insulator transition. However, the chemical potential is often found pinned at the top of the valence band or at the bottom of the conduction band in real systems due to holelike or electronlike impurity and defect states, respectively.[18] Thus, an increase in the binding energy in the present case suggests the pinning of the chemical potential at the bottom of the conduction band, as expected in an electron-doped material. Interestingly, the chemical potential shift appears when ~200 K, much below the metal-insulator transition temperature of 265 K, suggesting a phase coexistence in this intermediate temperature range as found in TEM data.

Employing high-resolution photoemission, we investigated the evolution of the band gap with temperature carefully at many temperature points. To maintain clarity in the presentation, some of the representative spectra consistent with Ref. 7 and their symmetrized forms are shown in Figs. 4(d) and 4(e). The spectra exhibit two distinct sets below and above ~200 K, possessing a significantly different intensity at ~300 meV [see Fig. 4(d)], the temperature where the twinned phase started to dominate in the TEM results. The data at 300 K exhibit a finite density of states at ϵ_F, suggesting a metallic phase, as expected. The intensity at ϵ_F gradually reduces with a decrease in temperature, as shown in the inset of Fig. 4(d).

Interestingly, the finite intensity at ϵ_F persists below 260 K, *pseudogap phase*. A hard gap is observed below ∼200 K, where the chemical potential also starts shifting. The band gap is ∼150 meV at 130 K. Since the TEM results exhibit gradual dominance of the twinned phase below 190 K, it is clear that the twinned phase is a gapped insulator and the pseudogap at higher temperatures corresponds to a charge-ordered phase. The finite quasiparticle intensity in the temperature range of 200–265 K appearing from the charge-ordered phase is localized due to charge ordering, leading to an insulating resistivity. These conclusions also support the evolution of the normalized (at 300 K) intensity ratio of the main peak to the satellite with temperature, shown in Fig. 4(c). The sharp drop in the intensity ratio at ∼265 K indicates a sharp reduction in the intensity of the well-screened feature, which can be attributed to the localization of the charge carriers across the metal-insulator transition temperature.

The CO phase is usually observed in the intermediate and low bandwidth systems such as layered manganites,[19] either due to the dominance of the superexchange interaction over the double-exchange and/or Jahn-Teller interactions. A strong electron correlation was also observed to lead to a phase separation.[2,20] In the present case, the compound is a simple cubic, three dimensional, and one among large bandwidth systems. A significantly low carrier concentration (electron doped) in this large bandwidth system indicates the weak role played by the electron correlation. Various experimental probes ensured a weak distortion of the MnO_6 octahedra.[7] Thus, the direct observation of charge ordering and phase coexistence in this system is unusual. Most interestingly, a pseudogap is found to associate with the CO phase, which appears in an intermediate temperature range (not a ground state) coexisting with an insulating phase.

In summary, these experimental results reveal the signature of a pseudogap associated with the charge-ordered phase; a precursor of this phase appears above the transition temperature as observed in layered manganites and cuprates.[10] Ironically, the pseudogap persists below 265 K, where the sample is insulating and coexists with an insulating twinned phase. The observation of charge ordering in these large bandwidth systems and phase coexistence in an intermediate temperature range questions conventional thinking about the bandwidth dependence on the stabilization of charge ordering and reveals the complexity of the correlated systems, demanding further investigations.

K.M. thanks T. V. Ramakrishnan and A. Fujimori for useful discussions.

*kbmaiti@tifr.res.in

[1] J. B. Goodenough, Rep. Prog. Phys. **67**, 1915 (2004); J. M. D. Coey and M. V. S. von Molnaacuter, Adv. Phys. **48**, 167 (1999); M. B. Salamon and M. Jaime, Rev. Mod. Phys. **73**, 583 (2001); Y. Tokura, Phys. Today **56** (7), 50 (2003); *Colossal Magnetoresistance, Charge Ordering and Related Properties of Manganese Oxides*, edited by C. N. R. Rao and B. Raveau (World Scientific Publishing, Singapore, 1998); T. V. Ramakrishnan, Curr. Sci. **95**, 1284 (2008).

[2] A. J. Millis, P. B. Littlewood, and B. I. Shairman, Phys. Rev. Lett. **74**, 5144 (1995).

[3] J. G. Bednorz and K. A. Muller, Z. Phys. B **64**, 189 (1986).

[4] R. E. Peierls, Ann. Phys. (Leipzig) **4**, 121 (1930).

[5] J. Hemberger, A. Krimmel, T. Kurz, H. A. KrugvonNidda, V. Y. Ivanov, A. A. Mukhin, A. M. Balbashov, and A. Loidl, Phys. Rev. B. **66**, 094410 (2002).

[6] O. Chmaissem, B. Dabrowski, S. Kolesnik, J. Mais, J. D. Jorgensen, and S. Short, Phys. Rev. B. **67**, 094431 (2003).

[7] R. Bindu, K. Maiti, R. Rawat, and S. Khalid, Appl. Phys. Lett. **92**, 121906 (2008); R. Bindu, G. Adhikary, S. K. Pandey, S. Patil, and K. Maiti, New J. Phys. **12**, 033026 (2010).

[8] R. Bindu, Eur. Phys. J. B **37**, 321 (2004).

[9] H. Fujishiro, T. Fukase, and M. Ikebe, J. Phys. Soc. Jpn. **67**, 2582 (1998).

[10] A. Kanigel, M. R. Norman, M. Randeria, U. Chatterjee, S. Souma, A. Kaminski, H. M. Fretwell, S. Rosenkranz, M. Shi, T. Sato, T. Takahashi, Z. Z. Li, H. Raffy, K. Kadowaki, D. Hinks, L. Ozyuzer, and J. C. Campuzano, Nat. Phys. **2**, 447 (2006); N. Mannella, W. L. Yang, X. J. Zhou, H. Zheng, J. F. Mitchell, J. Zaanen, T. P. Devereaux, N. Nagaosa, Z. Hussain, and Z.-X. Shen, Nature (London) **438**, 474 (2005); K. Maiti, R. S. Singh, V. R. R. Medicherla, S. Rayaprol, and E. V. Sampathkumaran, Phys. Rev. Lett. **95**, 016404 (2005); V. R. R. Medicherla, S. Patil, R. S. Singh, and K. Maiti, Appl. Phys. Lett. **90**, 062507 (2007); R. Bindu, K. Maiti, S. Khalid, and E. V. Sampathkumaran, Phys. Rev. B **79**, 094103 (2009).

[11] S. A. Kivelson, E. Fradkin, and V. J. Emery, Nature (London) **393**, 550 (1998); V. Hinkov, P. Bourges, S. Pailhès, Y. Sidis, A. Ivanov, C. D. Frost, T. G. Perring, C. T. Lin, D. P. Chen, and B. Keimer, Nat. Phys. **3**, 780 (2007); V. Hinkov, D. Haug, B. Fauqué, P. Bourges, Y. Sidis, A. Ivanov, C. Bernhard, C. T. Lin, and B. Keimer, Science **319**, 597 (2008).

[12] S. Doniach and M. Šunjić, J. Phys. C **3**, 285 (1970).

[13] S. W. Han, J. D. Lee, K. H. Kim, H. Song, W. J. Kim, S. J. Kwon, H. G. Lee, C. Hwang, J. I. Jeong, and J.-S. Kang, J. Korean Phys. Soc. **40**, 501 (2002); A. Sekiyama, S. Kasai, M. Tsunekawa, Y. Ishida, M. Sing, A. Irizawa, A. Yamasaki, S. Imada, T. Muro, Y. Saitoh, Y. Onuki, T. Kimura, Y. Tokura, and S. Suga, Phys. Rev. B **70**, 060506(R) (2004); H. Kumigashira, K. Horiba, H. Ohguchi, K. Ono, M. Oshima, N. Nakagawa, M. Lippmaa, M. Kawasaki, and H. Koinuma, Appl. Phys. Lett. **82**, 3430 (2003).

[14] R. S. Singh and K. Maiti, Phys. Rev. B **76**, 085102 (2007).

[15] K. Horiba, M. Taguchi, A. Chainani, Y. Takata, E. Ikenaga, D. Miwa, Y. Nishino, K. Tamasaku, M. Awaji, A.Takeuchi, M.Yabashi, H. Namatame, M. Taniguchi, H. Kumigashira, M. Oshima, M. Lippmaa, M. Kawasaki, H. Koinuma, K. Kobayashi, T. Ishikawa, and S. Shin, Phys. Rev. Lett. **93**, 236401 (2004).

[16] K. Maiti, U. Manju, S. Ray, P. Mahadevan, I. H. Inoue, C. Carbone, and D. D. Sarma, Phys. Rev. B **73**, 052508 (2006); K. Maiti, A. Kumar, D. D. Sarma, E. Weschke, and G. Kaindl, *ibid.* **70**, 195112 (2004); K. Maiti and D. D. Sarma, *ibid.* **61**, 2525 (2000); K. Maiti, D. D. Sarma, M. J. Rozenberg, I. H. Inoue, H. Makino, O. Goto, M. Pedio, and R. Cimino, Europhys. Lett. **55**, 246 (2001).

[17]P. G. Steeneken, L. H. Tjeng, G. A. Sawatzky, A. Tanaka, O. Tjernberg, G. Ghiringhelli, N. B. Brookes, A. A. Nugroho, and A. A. Menovsky, Phys. Rev. Lett. **90**, 247005 (2003); A. Fujimori, K. Morikawa, A. Ino, and T. Mizokawa, J. Electron Spectrosc. Relat. Phenom. **78**, 31 (1996); K. Maiti, J. Fink, S. de Jong, M. Gorgoi, C. Lin, M. Raichle, V. Hinkov, M. Lambacher, A. Erb, and M. S. Golden, Phys. Rev. B **80**, 165132 (2009); N. Harima, J. Matsuno, A. Fujimori, Y. Onose, Y. Taguchi, and Y. Tokura, *ibid.* **64**, 220507(R) (2001).

[18]A. Ino, T. Mizokawa, A. Fujimori, K. Tamasaku, H. Eisaki, S. Uchida, T. Kimura, T. Sasagawa, and K. Kishio, Phys. Rev. Lett. **79**, 2101 (1997); K. Maiti and D. D. Sarma, Phys. Rev. B **58**, 9746 (1998); **65**, 174517 (2002).

[19]Q. A. Li, K. E. Gray, S. N. Ancona, H. Zheng, S. Rosenkranz, R. Osborn, and J. F. Mitchell, Phys. Rev. Lett. **96**, 087201 (1996); H. Zheng, Q. A. Li, K. E. Gray, and J. F. Mitchell, Phys. Rev. B **78**, 155103 (2008).

[20]D. D. Sarma, D. Topwal, U. Manju, S. R. Krishnakumar, M. Bertolo, S. La Rosa, G. Cautero, T. Y. Koo, P. A. Sharma, S.-W. Cheong, and A. Fujimori, Phys. Rev. Lett. **93**, 097202 (2004).